Materials Today Bio 31 (2025) 101597

Contents lists available at ScienceDirect

Materials Today Bio

journal homepage: www.journals.elsevier.com/materials-today-bio

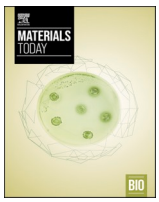

Targeting capture and eradicate circulating tumor cells by activated platelet derived vehicle for inhibiting triple-negative breast cancer metastasis

Hongmei Zhang [a,b,g,1], Jinlan Jiao [a,1], Yongxuan Long [a,1], Lina Zhou [b], Yinhua Lv [b], Wenqian Wei [b], Yuxiang Sun [e], Hao Han [c], Changrong Chen [d,*], Yun Zhu [a,b,f,**], Weijie Zhang [a,***]

[a] Division of Breast Surgery, Department of General Surgery, Nanjing Drum Tower Hospital, Affiliated Hospital of Medical School, Nanjing University , Nanjing, 210000, China
[b] Nanjing Drum Tower Hospital Clinical College of Traditional Chinese and Western Medicine, Nanjing University of Chinese Medicine, Nanjing, 210000, China
[c] Department of Ultrasound, Nanjing Drum Tower Hospital, The Affiliated Hospital of NanJing University Medical School, Nanjing, 210000, China
[d] Department of Emergency Surgery, Nanjing Drum Tower Hospital, Affiliated Hospital of Medical School, Nanjing University, Nanjing, 210000, China
[e] Jiangsu Key Laboratory of Integrated Traditional Chinese and Western Medicine for Prevention and Treatment of Senile Diseases, Institute of Translational Medicine, Medical College, Yangzhou University, Yangzhou, 225001, China
[f] Nanjing Medical Center for Clinical Pharmacy, Nanjing, Jiangsu, 210000, China
[g] Gansu Wuwei Institute of Medical Sciences, Gansu, 733000, China

ARTICLE INFO

Keywords:
Triple-negative breast cancer
Circulating tumor cells
Doxorubicin
Platelet membranes
Metastasis

ABSTRACT

Circulating tumor cells (CTCs) are cardinal intermediaries in the metastatic cascade, particularly in triple-negative breast cancer (TNBC), owing to their high-affinity interactions that bolster survival and dissemination. Addressing this pivotal mechanism, we have developed APEVs@DOX, a pioneering biomimetic delivery system. Utilizing activated platelet membranes as a scaffold, APEVs@DOX recapitulates the natural affinity between platelets and CTCs, enabling targeted delivery of doxorubicin. Our results, substantiated by meticulous *in vitro* and *in vivo* experimentation, revealed 78 % reduction in lung metastasis nodules in murine models relative to controls, affirming APEVs@DOX's proficiency in CTCs capture and eradication. This study not only illuminates the potential of CTCs-targeted therapies in the precision medicine armamentarium for TNBC but also contributes empirical data to guide the strategic design of anti-metastatic interventions. The therapeutic impact of APEVs@DOX in curtailing metastatic spread offers a beacon of hope for advancing TNBC treatment paradigms.

1. Introduction

Triple-negative breast cancer (TNBC) represents a significant challenge in oncology, primarily due to its high mortality rate, which is largely attributed to delayed diagnosis [1]. Early detection is crucial for reducing cancer-related deaths and improving patient outcomes. However, TNBC is known for its propensity for early metastasis, even more so than human epidermal growth factor receptor-2 positive or hormone receptor-positive tumors. Consequently, patients with TNBC face a median survival of only 12–18 months [2,3]. Hematogenous dissemination, the primary route for metastasis, brings circulating tumor cells (CTCs) into focus [4]. First hypothesized in 1960, CTCs have since become central to cancer research [5]. These cells, whether solitary or in clusters, possess high metastatic potential, with their presence indicating a poor prognosis in various cancers [6].

CTCs, shed from primary tumors into the bloodstream, act as seeds

* Corresponding author. Department of Emergency Surgery, Nanjing Drum Tower Hospital, Affiliated Hospital of Medical School, Nanjing University, Nanjing, 210000, China.
** Corresponding author. Nanjing Drum Tower Hospital, Affiliated Hospital of Medical School, Nanjing University, Nanjing, 210000, China.
*** Corresponding author. Division of Breast Surgery, Department of General Surgery, Nanjing Drum Tower Hospital, Affiliated Hospital of Medical School, Nanjing University, Nanjing, 210000, China.
E-mail addresses: changrongchen@163.com (C. Chen), njglyyzhuy@cpu.edu.cn (Y. Zhu), zhangweijie1616@nju.edu.cn (W. Zhang).
[1] These authors contributed equally to this work.

https://doi.org/10.1016/j.mtbio.2025.101597
Received 22 December 2024; Received in revised form 5 February 2025; Accepted 18 February 2025
Available online 21 February 2025

for distant metastases and are a critical element in the metastatic cascade [1,7]. Despite being recognized for over a century, isolating viable CTCs remains challenging due to their rarity in the vast number of blood cells [8]. For example, the detection of CTCs in early-stage breast cancer (stages I–IIIA)-more than one in 20 % of stage I, 26.8 % of stage II, and 26.7 % of stage III patients-highlights their elusive nature and underscores the need for targeted capture strategies[9–11]. Beyond their solitary existence, CTCs often form clusters, significantly enhancing their metastatic potential by 23–50 times compared to single cells [12]. Current research has already demonstrated the specific capture and neutralization of circulating tumor cells in the bloodstream through the high-affinity interactions between cancer cell membranes and homologous exosome membranes, thereby reducing tumor metastasis [13].

Specially, the interaction with platelets is crucial for successful hematogenous metastasis, facilitating this potentiation. Tumor cells activate platelets, leading to aggregation and adhesion, which creates a protective shield for CTCs survival *in vivo*. The translocation of P-selectin from α-granules to the platelet surface facilitates the binding of platelets to tumor cells, mediated by glycoprotein receptors and other adhesion molecules, fostering a conducive microenvironment for metastasis [14–17]. Leveraging the unique affinity between platelets and tumor cells, our approach innovatively explores CTCs targeted therapeutic strategies by platelet derived vesicles. This avenue, supported by academic consensus, invites further investigation into the interactions between platelets and tumors for developing advanced, targeted cancer treatments.

Cell membrane-coated platforms have emerged as a promising platform for biomedical applications, offering properties similar to their source cells, such as biocompatibility, immune evasion, and tumor tropism[18–20]. Platelet membranes have a wide range of functions and are frequently used in anti-tumor treatments. Engineered platelets, due to their intrinsic ability to target bleeding sites, possess the function of reducing the recurrence rate of cancer after surgery [21–23]. Utilizing the adhesion dynamics between CTCs and platelets, our study introduces an activated platelet membrane-based biomimetic platform to capture CTCs and deliver cytotoxic drug doxorubicin (APEVs@DOX) for inhibiting CTCs related metastasis. Firstly, constructed using the supernatant from TNBC medium to activate platelet cells, this platform targets the delivery of Adriamycin to CTCs. Through *in vitro* and *in vivo* evaluations, we assess the affinity of APEVs@DOX towards TNBC cells, the enhancement of doxorubicin's efficacy, and the efficiency in capturing CTCs and inhibiting metastasis. This integrated approach aims to delineate the specificity of activated platelet cell biomimetics in targeting TNBC and their pivotal role in intercepting CTCs, which are critical for metastatic spread, thereby offering a transformative solution to the challenges posed by CTCs in TNBC therapy (see Scheme 1).

2. Materials and methods

2.1. Microarray data

The functional genomics data repository GEO (http://www.ncbi.nlm.nih.gov/geo) is accessible to the public and contains high throughput gene expression data, chips, and microarrays [24]. We downloaded three gene expression datasets [GSE183635, GSE68086, and GSE18893] from GEO (Affymetrix Human Genome U133 Plus 2.0 Array and Affymetrix GPL570 platform). Based on the annotation data on the platform, the probes were translated into the appropriate gene symbol. There were 90 BC Platelets samples and 105 platelets from healthy volunteers in the GSE183635 dataset. 39 BC platelet samples and 55 platelet samples from healthy volunteers were present in GSE68086. GSE188893 comprised 13 primary tumor samples, which included parental cell lines and primary tumor nodules, and 10 CTCs/DTC samples in the MDA-MB-231 xenograft model.

2.2. Identification of DEGs

Using GEO2R (http://www.ncbi.nlm.nih.gov/geo/geo2r), the DEGs were examined. Using an interactive web application called GEO2R, users may compare two or more datasets within a GEO series to find

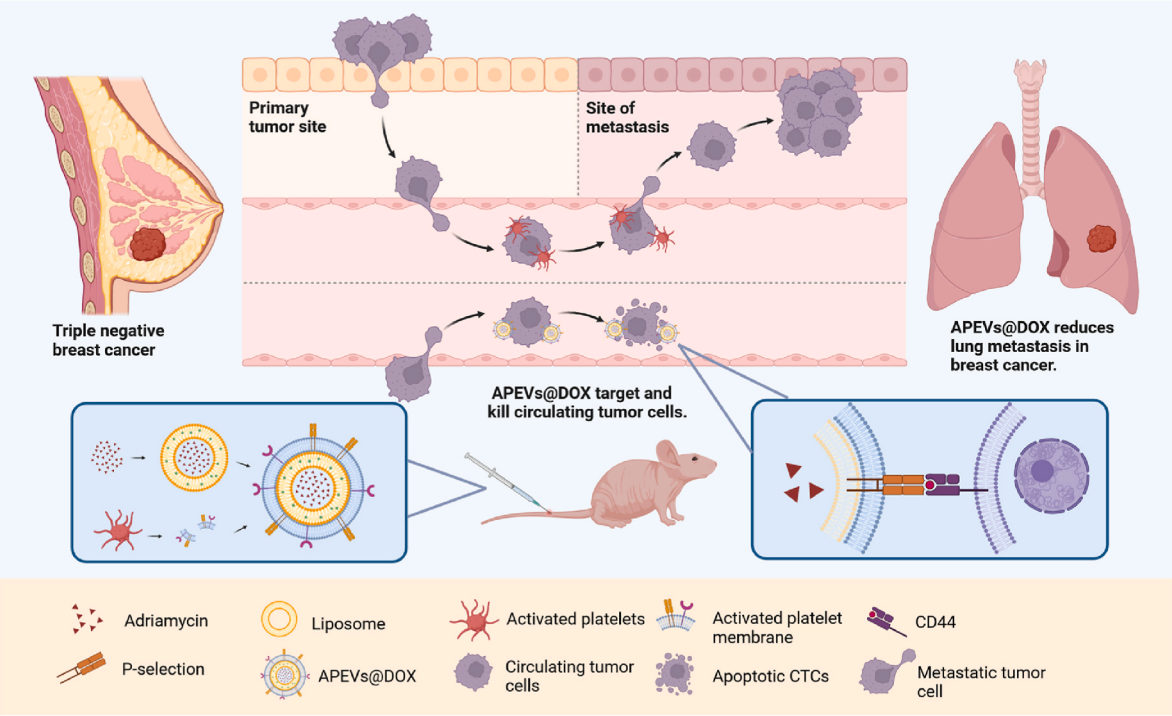

Scheme 1. The schematic illustrates the key role of circulating tumor cells in the metastasis of triple-negative breast cancer and highlights the use of platelet-membrane biomimetic platform to capture and kill CTCs by delivering drugs, ultimately reducing lung metastasis. The interaction between CTCs and the APEVs@DOX, driven by their high affinity, is emphasized as a critical step in preventing the spread of the tumor.

DEGs under various experimental circumstances. Applying Benjamini and Hochberg's false discovery rate and adjusted P-values (adj.P) allowed for a compromise between the potential for false positives and the identification of statistically important genes. Genes having more than one probe set or probe sets lacking matching gene symbols were averaged or eliminated accordingly. Statistical significance was defined as adj. P-values <0.01 and logFC (fold change) > 1.

2.3. GO enrichment analyses of DEGs

An online biological information database called the Database for Annotation, Visualization, and Integrated Discovery (DAVID; http://david.ncifcrf.gov) combines biological data and analysis tools to give users access to a comprehensive set of functional annotation information about genes and proteins, allowing them to extract biological information [25]. Gene Ontology (GO) is a prominent bioinformatics tool for gene annotation and biological process analysis [26]. Biological investigations were carried out utilizing the DAVID online database to examine the role of DEGs. Statistics were deemed significant if $P < 0.05$.

2.4. PPI network construction and module analysis

Using the Search Tool for the Retrieval of Interacting Genes (STRING; http://string-db.org) (version 10.0) online database, the PPI network was predicted [27]. Examining how proteins interact functionally can shed light on the processes involved in the emergence or progression of illnesses. An interaction with a combined score > 0.4 was deemed statistically significant in the current study, which built the PPI network of DEGs using the STRING database. Cytoscape is an open-source bioinformatics software for visualizing molecular interaction networks (version 3.4.0) [28]. Cytoscape was used to draw the PPI networks and identify their most important module.

2.5. Hub genes analysis

Degrees of selection ≥ 1 were used for the hub genes. The Kaplan-Meier curve from the Kaplan-Meier Plotter online database (http://kmplot.com/analysis/) was used to do the hub gene analyses for overall survival and disease-free survival, with the optimal cutoff value being chosen automatically. The expression levels of these seven genes in various cancers were examined using the TIMER database.

2.6. Materials

Unless otherwise stated, all chemicals were purchased from commercial suppliers (Beyotime Biotechnology and Thermo Fisher Scientific) and used as received without further purification. Cholesterol, 1,2-dipalmitoyl-sn-glycero-3-phosphocholine(DMPC), and Coumarin 6 were purchased from Shanghai Yuanye Bio-Technology Co., Ltd. Reagents Doxorubicin was obtained from Shanghai Aladdin Biochemical Technology Co.,Ltd. Hoechst 33,342 was purchased from KeyGEN BioTECH (Nanjing, China). Mouse anti-p-selectin, Alexa488 goat anti-rabbit IgG (H + L), and Mouse anti-β-actin (60008-1-Ig) were purchased from Proteintech. Goat anti-Rabbit Ig(H&L)-HRP and Goat anti-Mouse Ig(H&L)-HRP were purchased from Bioworld Technology CO., Ltd. Trypsin, phosphate-buffered saline (PBS), Fetal bovine serum (FBS), and DMEM were obtained from SenBeiJia Biological Technology Co., Ltd. All other chemicals and reagents e of analytical grade and without further purification. Deionized water (18.2 MΩ cm) from a Milli-Q purification system was used in all preparations.

2.7. Cell lines and cell culture

Human breast cancer cells (MDA-MB-231) and mouse embryonic fibroblasts (3T3) were purchased from the cell bank of the Shanghai Institute of Biochemistry and Cell Biology, Chinese Academy of Sciences. Cell lines were cultured in DMEM supplemented with 10 % fetal bovine serum (FBS) and penicillin-streptomycin solution (Biochannel, Nanjing, China). All cells were cultured in an incubator with 5 % CO2 at 37 °C. Cells were stored at −80 °C. Cells were maintained, and experiments were conducted at cell densities that allowed exponential growth or otherwise mentioned.

2.8. Platelet membrane preparation and characterization

Human platelet-rich plasma (PRP) was donated from healthy volunteers with permission from the Ethics Committee of the Affiliated Drum Tower Hospital of Nanjing University Medical School by the Declaration of Helsinki. Briefly, blood was collected using sodium citrate anticoagulation tubes and centrifuged at 800 rpm for 10 min at room temperature to obtain platelet-rich plasma (PRP). Then PRP was centrifuged at $1800\times g$ for 12 min twice, and the supernatant was discarded. The obtained pellet was gently rinsed with D-hanks to prepare purified platelets. All experiments were performed under sterile conditions. The purified platelets obtained were split in two; one was immediately frozen in a −80 refrigerator, and the other was incubated with thrombin for 30 min at room temperature on a shaker with an addition of protease inhibitor and stored at −80 °C. Platelet activation was measured by flow cytometry before freezing and after thrombin incubation.

A repeated freeze-thaw process derived the platelet membrane. The platelet incorporating protease inhibitors was frozen at −80 °C, thawed at 4 °C, and pelleted by centrifugation at 21,100 g for 10 min. The pellet was then resuspended in the lysis buffer, and the freeze-thaw was repeated two more times. After the repeated washes, the membrane was suspended in water for coating onto the nanoparticle cores. PEVs@DOX was produced by mixing the above lipo@dox with platelet membranes and then simply sonicated.

Quantification of total membrane protein concentration was performed using a Pierce BCA protein assay kit (Life Technologies). Flow cytometry was used to probe for the expression of specific surface markers on the platelet membrane using Alexa488-conjugated goat anti-rabbit IgG (H + L) and anti-human P-selectin (AK4; Biolegend). The probes (1:200 dilution) were incubated with a purified platelet in D-hanks for 30 min in the dark at room temperature. After incubation, Data were collected using a Becton Dickinson Accuri Dil flow cytometer equipped with BD Accuri Dil Plus software and analyzed with FlowJo V10 software.

2.9. Preparation of LP nanoparticles (NPs)

Liposomal doxorubicin is prepared using the thin film dispersion method. Simply dissolve DMPC and cholesterol in anhydrous ethanol at a ratio of 4:1, evaporate the organic solvent under reduced pressure, and slowly hydrate the resulting lipid film solution with doxorubicin hydrochloride solution dissolved in deionized water (drug/lipid = 1:5–10 mass ratio). The obtained solution was treated with ultrasound (30 s, on 3 S off 2 s, 60 % W), then stirred and incubated at 55 °C, 1000 rpm for 2 h, washed and centrifuged twice with an ultrafiltration tube to obtain liposome adriamycin solution.

APEVS@DOX and NAPEVS@DOX were prepared by mixing the above-prepared 0.4 mg lipo@DOX with activated and inactive platelet membranes extracted from 1 ml of blood. Respectively, and then treated with ice bath ultrasound (2 min, on 3 S off 2 s, 25 % W).

2.10. Characterization of nanoparticles

Transmission electron microscopy (TEM) visualized the nanoparticles' morphology at various stages. Tutions and zeta potentials of the nanoparticles were evaluated using a 90Plus/BI-MAS instrument (Brookhaven Instruments Co., U.S.A.). The UV/Vis absorption spectra and the Fourier transform infrared (FTIR) spectra were measured with a

Varian 4000 UV–Vis spectrophotometer and a Varian 3000 FTIR spectrophotometer, respectively. The membrane proteins of Lipo@DOX, APLTM, APEVs@DOX, NAPLTM, and NAPEVs@DOX were analyzed by SDS-PAGE.

Accurately weigh a fixed amount of doxorubicin hydrochloride and use ultrapure water to prepare standard solutions of doxorubicin hydrochloride with concentrations of 0.1 μg/mL, 0.5 μg/mL, 1 μg/mL, 1.5 μg/mL, 2 μg/mL, and 2.5 μg/mL. Measure the fluorescence values at excitation and emission wavelengths of 495 nm and 595 nm, respectively, using a multifunctional microplate reader to construct a standard curve for doxorubicin hydrochloride solution.

For the determination of drug encapsulation efficiency (Drug encapsulation efficiency, EE%) and drug loading capacity (Drug loading capacity, DL%): Take 200 μL of the liposome solutions of lipo@DOX, NAPEVs@DOX and APEVs@DOX, respectively, and dissolve them in 2 mL of methanol. Sonicate in a water bath for 30 min, and then measure the absorbance using a UV spectrophotometer. Calculate the drug concentration based on the aforementioned standard curve.

Calculation formulas:

Encapsulation efficiency (EE%) = (Measured concentration of doxorubicin in drug-loaded nanoparticles × Solution volume)/Drug input × 100 %

Drug loading capacity (DL%) = (Measured concentration of doxorubicin in drug-loaded nanoparticles × Solution volume)/Total drug amount in the system × 100 %

2.11. Western blotting assay

Cells were lysed using RIPA buffer (P0013B, Beyotime) supplemented with protease inhibitor cocktail (P1005, Beyotime) and PMSF (ST507-10 mL, Beyotime) and then centrifuged at 12,000 g for 12 min. The supernatant collected was subjected to protein content determination by the BCA method, and the protein samples prepared as described above were subjected to polyacrylamide gel electrophoresis; after electrophoresis, the protein bands were transferred to nitrocellulose membranes. After the blotted membranes were blocked for 2 h, they were incubated with the indicated primary antibody (60008-1-Ig/60322-1-Ig/28083-1-AP, Proteintech, 1:10000/1:10000/1:6000) overnight at 4 °C and then incubated with HRP-conjugated secondary antibodies (SA00001-1, Proteintech, 1:20000) for 1 h. Finally, the signal intensity is read and analyzed by ECL chemiluminescence.

2.12. Cellular uptake

The MDA-MB-231 cells were grown on the coverslips. Then, Dil-labeled NAPEVs@DOX and APEVs@DOX (Dil, 10 μM) were added to the cells for 4 h of incubation. After that, cell nuclei were stained with Hoechst 33342 after washing and fixing with 4% paraformaldehyde. Finally, the cellular uptake efficiency was captured by a CLSM(Leica Microsystems Ltd.). To investigate cellular uptake of APEVs@DOX by p-selectin receptors on the cell surface, MDA-MB-231 cells cultured without serum were preincubated with anti-p-selectin antibody for 1 h to block p-selectin receptors. Then, the cells were washed and incubated with Dil-labeled APEVs@DOX (Dil, 10 μM) for another 6 h. The Dil fluorescence was observed by a CLSM, and the cellular uptake efficiency was also detected by flow cytometry.

2.13. In vitro cytotoxicity

3T3 cells were inoculated in 96-well plates at a density of 7×10^3 wells, incubated overnight with 5 % CO_2 at 37 °C, and then treated with PBS and liposome solutions with different concentrations for 48 h. The cell activity was determined with MTT.

2.14. Hemolysis test

Different preparations were made using a specific concentration gradient solution with normal saline. Fresh whole blood was collected in an anticoagulant centrifuge tube and centrifuged at 3500 rpm for 15 min to obtain red blood cells (RBCs). Every 200 μL of blood precipitation was suspended and diluted with normal saline to 10 mL, and an RBC reserve solution with a concentration of 2 % was prepared. Different groups of preparations were mixed with red blood cells and incubated, and deionized water and normal saline were used as positive and negative controls, respectively. The samples were incubated at 37 °C for 1 h and centrifuged at 1000 rpm for 10 min to observe hemolysis and take photos for record. Take the supernatant to measure the absorbance at 545 nm, and calculate the hemolysis rate as follows: Hemolysis rate (%) = (Asample-Anegative)/(Apositive-Anegative) *100 %.

2.15. Wound healing assay

The MDA-MB-231 cells were spread in 6-well plates at a density of 1×10^6/mL per well, and after overnight incubation, Confluent cells were scratch wounded and incubated with PBS, DOX, NAPEVs@DOX and APEVs@DOX (DOX:1.5 μg/mL). The cell migration status was assessed over 48 h and documented by microscopic photographs at the indicated time points.

2.16. Transwell assay

The invasion and migration abilities of the cells were evaluated using Transwell chambers with 8 μm pore filters. Cells (1.5×10^4/100 μL) were seeded on the upper chambers coated in serum-free DMEM and treated with different treatments. DMEM containing 10 % FBS was added to the lower chambers. After incubation for 24 h at 37 °C, the cells in the chambers were collected and fixed with 4 % paraformaldehyde. After removing the nonmigrating or noninvading cells with cotton swabs, the chambers were stained with crystal violet solution for 20 min. The results were recorded at × 200 magnification under a microscope. All assays were repeated three times in duplicate.

2.17. Mouse model of BC lung metastasis

All animal experiment protocols using mice were approved by the Animal Ethics Committee of Nanjing First Hospital (Nanjing, China). The methods were carried out according to the relevant guidelines, including any relevant details. The athymic female BALB/c-nude mice (4–6 weeks, 16–20 g in body weight) were purchased from GemPharmatech Co., Ltd. They were kept in specific pathogen-free (SPF) conditions with controlled temperature (23 ± 2 °C) and humidity (60 % ± 5 %), a 12 h light/dark cycle, and free access to water and food. Treated cells (1×10^6/150 μL PBS) were injected through the tail vein of the nude mice. Pulmonary metastasis was evaluated by bioluminescence imaging at 4 or 8 weeks. Then, the mice were sacrificed, and the lung tissues were imaged and fixed in 4 % paraformaldehyde for further analysis. All animal procedures were carried out ethically and humanely.

2.18. Haematoxylin and eosin (HE) and immunohistochemical (IHC) staining

HE and IHC staining followed the standard protocols described in a previous study [29]. The results of IHC staining were evaluated considering both the staining intensity and the proportion of tumor cells.

2.19. Immunofluorescence (IF) assay

To assess the anti-tumor efficacy of nanoparticles, live cell staining was performed on MDA-MB-231 breast cancer cells. Cells were seeded at

2×10^3 cells/well in 12-well plates and incubated overnight at 37 °C, 5 % CO_2. Experimental groups received 6 μg/mL adriamycin treatment for 48 h. After discarding the medium and washing with PBS, 200 μL Calcein-AM was added per well and incubated at 37 °C in the dark for 30 min. Cells were then washed with PBS and observed under a fluorescence microscope (Calcein-AM: green fluorescence, Ex/Em = 494/517 nm).

2.20. Biosafety assessment

The major organs after antitumor efficacy evaluation were collected for tissue histological examination (H&E staining).

2.21. Statistical analysis

All data were reported as the mean ± standard deviation (SD) or the mean ± standard error of the mean (SEM) of at least three samples. One-way analysis of variance (ANOVA) and Tukey's post hoc tests were used in multiple comparisons. All statistical analyses were carried out using GraphPad PRISM 5 software. P values of <0.05, <0.01, and <0.001 are accepted as indicative of significant differences.

3. Results and discussion

3.1. Correlation between CTCs and platelets in TNBC metastasis

To explore the correlation between platelet cells and CTCs, we conducted comprehensive bioinformatics analyses. This approach allowed us to delve into the underlying molecular interactions and identify potential pathways that may contribute to the affinity between platelets and CTCs. After standardizing the microarray results, differential expression genes (DEGs) were identified between paired normal and breast cancer samples in CTCs and tumor-educated platelets. Specifically, we identified 1595 DEGs in GSE183635, 7447 in GSE68086, and 1882 in GSE18893. The overlap among these datasets revealed 98 intersection genes, as depicted in the Venn diagram (Fig. 1A). These 98 intersection genes are considered pivotal in influencing the interaction between CTCs and platelets. Functional and pathway enrichment analyses were performed using the Database for Annotation, Visualization and Integrated Discovery (DAVID) to classify the biological significance

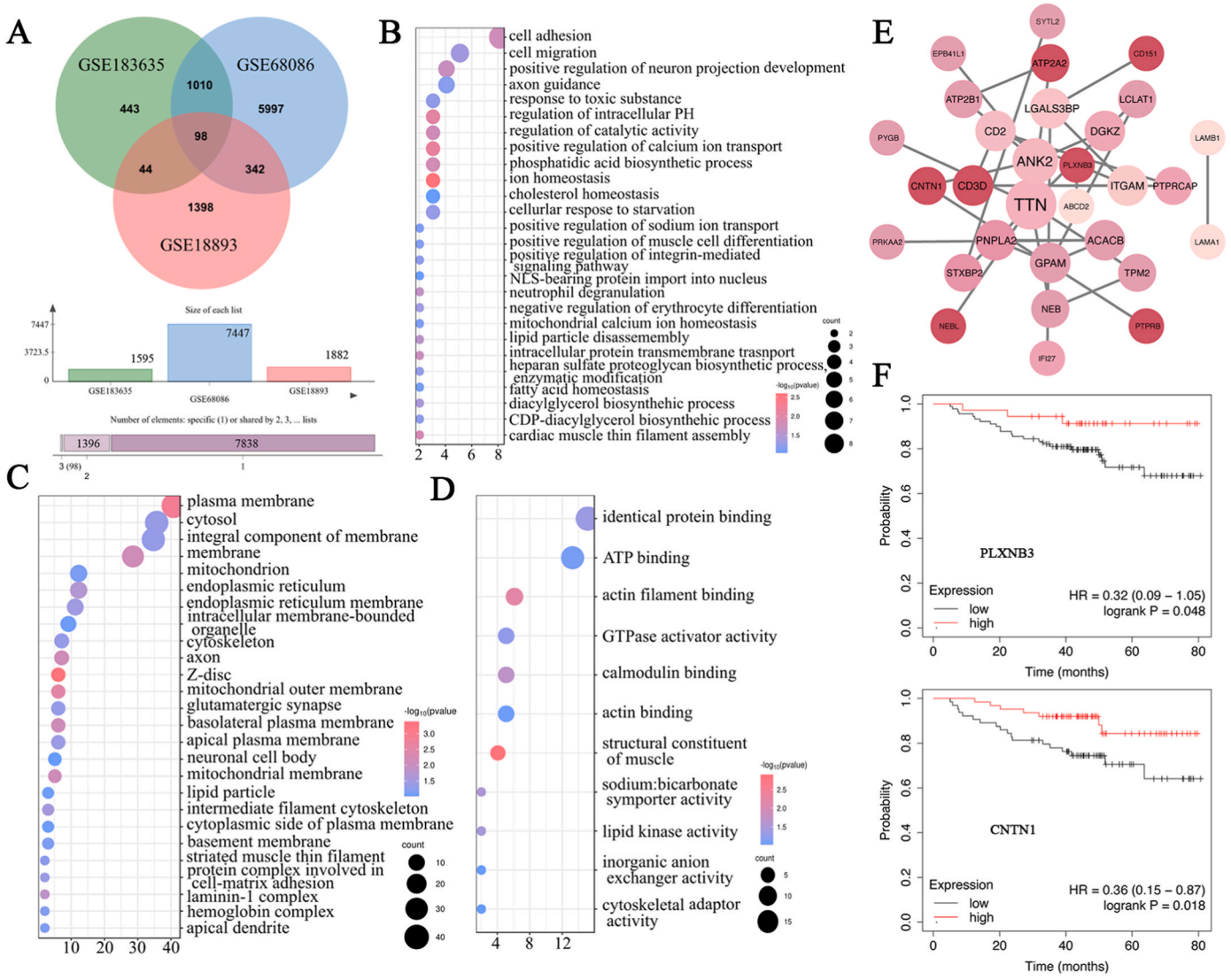

Fig. 1. Tumor cell-platelet interactions. (A) Overlap the differentially expressed genes of interest from GEO datasets (GSE183635, GSE68086 and GSE18893). (B–D) GO terms in biological process, cellular component, and molecular function were used for functional enrichment clustering analysis on common DEGs. (E) STRING Protein-Protein Interaction network is the most significant module of all genes enriched by the above gene functions. (F) Kaplan-Meier survival curves in TNBC patients.

of these DEGs. Gene Ontology analysis showed that the biological processes (BP) of DEGs were significantly enriched in cell adhesion, cell migration, and the positive regulation of neuron projection development (Fig. 1B). In terms of cellular components (CC), DEGs were mainly enriched in the plasma membrane, cytosol, and integral component of the membrane (Fig. 1C). For molecular functions (MF), DEGs were enriched in identical protein binding, ATP binding, actin filament binding, GTPase activator activity, and calmodulin binding (Fig. 1D). These findings align with existing literature [15,30,31], which indicates that tumor cells activate and adhere to platelets through membrane surface ligands, thereby enhancing the migratory capacity of tumor cells.

We then constructed a STRING Protein-Protein Interaction (PPI) network and identified the most significant module using the STRING database and Cytoscape software. This analysis yielded 30 genes with interaction relationships (Fig. 1E). Among these 30 genes, the expression of seven genes-PLXNB3, CD3D, CNTN1, ATP2A2, CD151, PTPRB, and NEBL-was associated with poor overall survival (OS) of TNBC patients, as shown by Kaplan-Meier Plotter datasets (Fig. 1F and Fig. S1). These seven genes are highlighted in bright red in Fig. 1E. Additionally, TIMER database analysis revealed that these genes were significantly differentially expressed across various tumor tissues, including Kidney Renal Papillary Cell Carcinoma (KIRP), Liver Hepatocellular Carcinoma (LIHC), Lung Adenocarcinoma (LUAD), Lung Squamous Cell Carcinoma (LUSC), and Prostate Adenocarcinoma (PRAD) (Fig. S2). In summary, the results above highlight a significant correlation between CTCs and platelets in the metastatic process of TNBC, underscoring the critical role of identified key differential expression genes in facilitating tumor cell adhesion and migration. In summary, the interaction between platelet cells and circulating tumor cells, as well as the associated genes, is closely related to the progression of TNBC.

3.2. Fabrication and characterization of activated platelet membrane-modified liposomes

Platelet cells are activated to form complexes with CTCs to promote the organ colonization during metastasis [32,33]. Therefore, activated platelet cell vesicles (APEVs) may be more advantageous for capturing CTCs, due to specific receptor-ligand interactions that facilitate targeted binding. Additionally, APEVs offer immune evasion capabilities, protecting the drug from rapid clearance, and prolonging the circulation time of the drug in the bloodstream to enhance sustained capture of CTCs. These attributes make PEVs an ideal vehicle for targeted drug delivery in the treatment of metastatic TNBC. Herein, the lipid-soluble compound DMPC was used to encapsulate the water-soluble anticancer agent Adriamycin, resulting in the liposomal delivery system Lipo@DOX. Platelets can be activated by co-incubation with thrombin. After activation, an increase in the level of CD62P is detected in platelets by flow cytometry (Fig. S3). Subsequently, platelet membranes are prepared by the freeze-thaw method. Prior to the modification of these liposomes with platelet membrane coatings, we ascertained the expression profile of proteins extracted from activated platelets. Western blot analyses revealed the conspicuous presence of p-selectin in the activated platelet extracts, whereas inactivated counterparts exhibited limited expression (Fig. 2C). Building upon this results, activated platelet membranes, recognized for their potential to augment drug delivery, were seamlessly integrated into the phospholipid bilayer of the liposomes via ultrasonication, giving rise to the APEVs@DOX formulation. To serve as a control, vesicles modified with inactivated platelet membranes were also fabricated, denominated as NAPEVs@DOX.

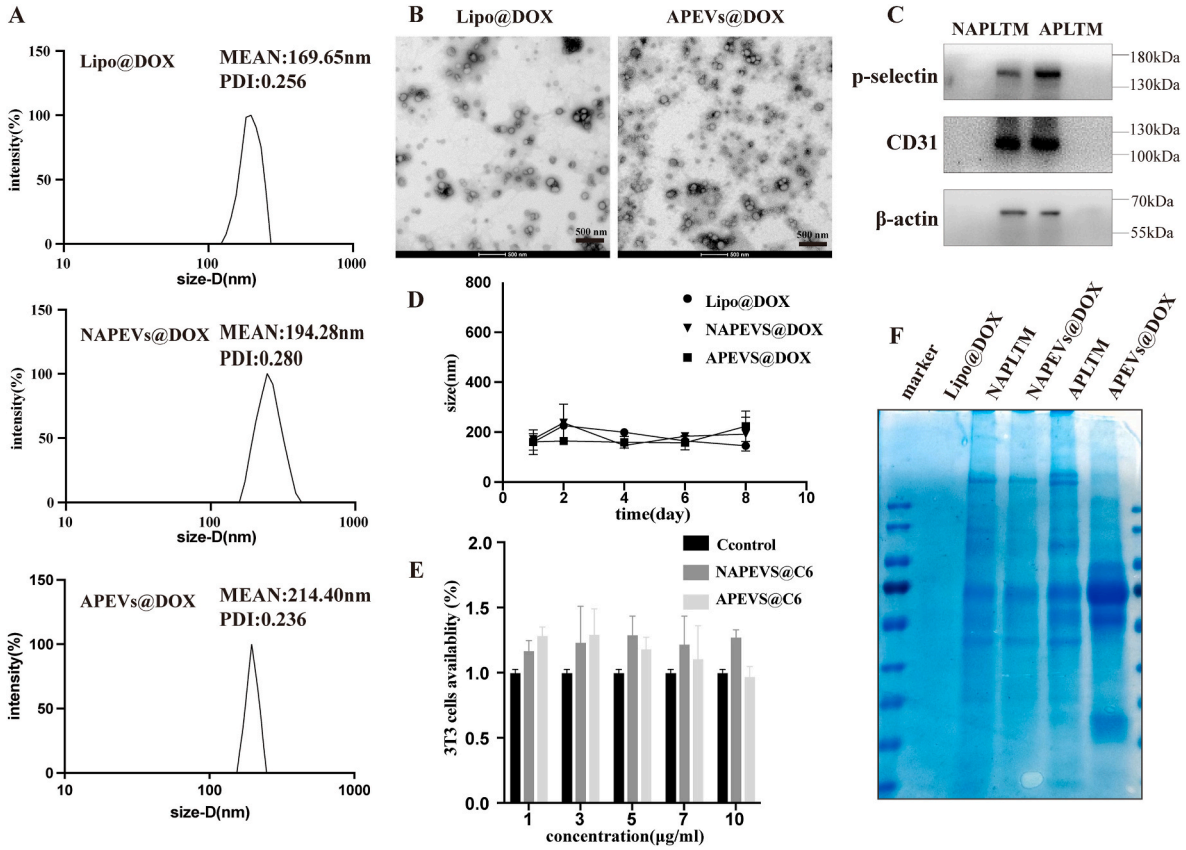

Fig. 2. Characterization of APEVs@DOX. (A) Hydrodynamic size and PDI of NAPEVs@DOX and APEVs@DOX. (B) Representative TEM image of Lipo@DOX and APEVs@DOX. (C) Determination of platelet activation and inactivation status by western blot. (D) Hydrodynamic size changes of Lipo@DOX, NAPEVs@DOX, and APEVs@DOX within two weeks in water. (E) Safety evaluation of liposome solutions with different concentrations studied with 3T3 cells. (F) Protein content visualization of preparations.

Characterization of the vesicle formulations through dynamic light scattering (DLS) indicated hydrodynamic diameters averaging 169.65 nm (PDI, 0.256) for Lipo@DOX, 194.28 nm (PDI, 0.280) for NAPEVs@DOX, and 214.40 nm (PDI, 0.236) for APEVs@DOX (Fig. 2A). Transmission electron microscopy (TEM) images corroborated the aspherical and homogenous morphology of both NAPEVs@DOX and APEVs@DOX (Fig. 2B). We also measured the zeta potential of the drug-loaded nanoparticles. The results showed that the zeta potential of Lipo@DOX was -9.83 ± 1.11 mV, that of NAPEVs@DOX was -6.87 ± 0.77 mV, and that of APEVs@DOX was -5.64 ± 0.72 mV. Additionally, we determined the encapsulation efficiency (EE%) and drug loading capacity (DL%) of the drug-loaded nanoparticles. The EE% of Lipo@DOX was 68.75 %, and its DL% was 10.58 %. Both NAPEVs@DOX and APEVs@DOX had EE% values above 40 % and DL% values around 7 %(Table S1). Furthermore, long-term stability assessments underlined the commendable stability of APEVs@DOX in a NaCl solution for up to eight days (Fig. 2D), underscoring the potential of these engineered platelet vesicles to facilitate enhanced targeting of breast cancer metastases. The cytotoxicity profile of the liposomal formulations devoid of drug cargo was investigated following a 48 h incubation period with 3T3 cells. MTT assays conducted in triplicate revealed that cell viability across all concentration ranges remained consistently above 90 % (Fig. 2E), attesting to the biocompatibility and safety of the delivery vehicle. Additionally, hemolytic assays employing erythrocytes suspended in phosphate-buffered saline (PBS) at physiological pH (7.4) confirmed the non-hemolytic nature of the engineered vesicles, with distilled water serving as a positive control and physiological saline as a negative control, thus establishing the safety of the drug delivery system in the circulatory milieu (Fig. S4). We also conducted pharmacokinetic-related tests on APEVs@DOX (Fig. S5) and found that the plasma concentration of the formulation did not decrease as rapidly as reported for free DOX [19]. This indicates improved stability and prolonged circulation time of APEVs@DOX *in vivo*, which may contribute to its enhanced therapeutic efficacy.

To ascertain the targeted protein expression on the surface of the drug delivery systems, we conducted SDS-PAGE gel electrophoresis. The electrophoretic profiles revealed an absence of protein expression in the Lipo@DOX formulation, devoid of platelet membrane modifications. Conversely, the activated and inactivated platelet membrane-coated formulations mirrored the protein band patterns and molecular weight profiles of their respective unmodified platelet membrane controls (Fig. 2F), affirming the successful incorporation and retention of platelet membrane proteins post-engineering. These findings collectively underscore the achievement of our goal to develop a targeted drug delivery system with enhanced specificity towards breast cancer metastasis.

3.3. Investigating the targeted delivery efficacy and cellular uptake of APEVS@DOX in TNBC tumor cells

To evaluate the targeted delivery capabilities and cellular uptake of the nanoparticles modified with activated platelet membranes, we employed laser confocal scanning microscopy utilizing a Leica-SP8 STED microscope. Employing fluorescent dye APEVs@Dil for visualization purposes, we observed the interaction between the APEVs@Dil and the MDA-MB-231 cell line, a model for triple-negative breast cancer. Following a 6 h incubation period, the LCSM images revealed a pronounced co-localization of Dil within the MDA-MB-231 cells when treated with APEVs@Dil (Fig. 3A) in contrast to NAPEVs@Dil and Lipo@Dil. Moreover, the results from flow cytometry also reflected these findings(Fig. S6). A notable feature was the stronger fluorescent signal in the cytoplasm compared to the nucleus, indicative of efficient cellular internalization. This finding indicated the higher affinity of APEVs to MDA-MB-231 cells, confirming the potentials for targeting delivery of doxorubicin to TNBC cells.

Due to the high expression of some proteins including P-selectin in activated platelet cells[34–36], we first used P-selectin antibodies to competitively bind the cell receptors. We then proceeded with the cellular uptake experiments to validate the behavioral differences of vesicles from activated platelet cells. Cells were pre-incubated with the antibody for 1 h prior to treatment with APEVs@Dil at a concentration of 10 μM Dil equivalent for an additional 6 h period. The results depicted in Fig. 3A demonstrated a significant reduction in the cellular uptake of APEVs@Dil by MDA-MB-231 cells post-treatment with the P-selectin inhibitor. Quantitative analysis of the cellular uptake, performed using ImageJ software, further corroborated these observations. At the 6 h time point, the P-selectin inhibition significantly decrease the fluorescent signal intensity compared to untreated APEVs@Dil (Fig. 3B). This data substantiates the targeted delivery mechanism of APEVs@Dil, specifically towards cells expressing surface-bound P-selectin. Moreover, since Dox has fluorescent properties, we also conducted the same uptake experiments using DOX, Lipo@DOX, NAPEVs@DOX, and APEVs@DOX. The results were consistent with the previous findings. This further confirmed that our formulations could enhance the *in vitro* uptake efficiency of DOX (Fig. S7 and Fig. S8).

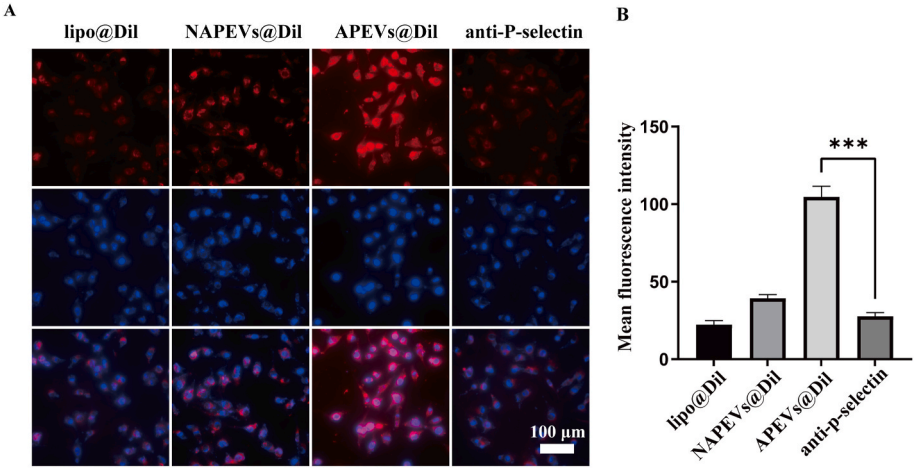

Fig. 3. Experimental evaluation of cell uptake efficiency of APEVs@Dil. (A) *In vitro* fluorescence microscopy images of different treatments in MDA-MB-231 cells after 6 h incubation. The nucleus was stained with Hoechst 33342 (blue). The vesicles were loaded with Dil (red). (B) Semiquantitative intracellular uptake of different treatments determined by the averaged Dil Fluorescence intensity in the Image J software. Scale bars: 100 μm. (For interpretation of the references to colour in this figure legend, the reader is referred to the Web version of this article.)

3.4. Evaluating the therapeutic efficacy and migration inhibition of APEVs@DOX in vitro

Recent studies have explored the effects of DOX in a mammary tumor spheroid (MTS) model. Results show that DOX enhances cytotoxicity in MTSs, reduces cell migration, and inhibits changes in E-cadherin and vimentin expression, which are characteristic of the epithelial-mesenchymal transition (EMT). These findings suggest that DOX may inhibit the metastatic process, warranting further investigation [37]. Moreover, DOX exposure for 24 h induces immunogenic cell death (ICD) by releasing damage-associated molecular patterns (DAMPs) and tumor antigens from cancer cells, which activate the immune system. This ICD induction forms the basis of an effective immunization strategy, preventing primary tumor formation and distant metastasis in preclinical breast cancer models [38].

To assess the therapeutic efficacy of APEVs for delivering drugs, doxorubicin (DOX) was encapsulated (APEVs@DOX) to conducted a series of experiments focusing on cell viability and migratory capacity on triple-negative breast cancer cells. To visually confirm the treatment outcomes, live cell staining was performed following 48 h of exposure to 6 μg/mL DOX. The efficacy of the free drug group is most pronounced, primarily due to the uptake mechanisms of doxorubicin hydrochloride in *in vitro* models, which aligns with findings from numerous DOX-related studies. Notably, the activated vesicle group APEVs@DOX exhibits significantly enhanced efficacy compared to its unactivated counterpart, suggesting that the expression of proteins on the cell membrane post-activation plays a pivotal role in therapeutic efficacy (Fig. 4A and B).

Given that epithelial-to-mesenchymal transition (EMT) plays a pivotal role in tumor progression, particularly in the colonization of vascular endothelial cells and subsequent distant metastasis[39–41], we explored the effects of APEVs@DOX on EMT-related processes. Since DOX doses below 2 μg/mL had minimal impact on cell proliferation, we selected a 1.5 μg/mL DOX concentration for further investigation of tumor cell migration inhibition. Utilizing Transwell assays, we assessed the migratory activity of metastatic MDA-MB-231 cells following 24 h incubation with free DOX, NAPEVs@DOX, and APEVs@DOX. The results showcased more than 80 % reduction in the migratory capacity of MDA-MB-231 tumor cells in the APEVs@DOX group (Fig. 4C) compared with control group, signifying the enhanced tumor-killing effect achieved through increased DOX uptake facilitated by the adhesion of activated platelet membranes.

Moreover, in cell scratch assays conducted at 24 and 48 h, we observed a lack of cell migration in the APEVs@DOX group, with the area of the cell-free region remaining virtually unchanged from the initial condition (Fig. 4E). Quantitative analysis of migrated cell counts in the Transwell assay and the non-migrated area in the cell scratch assay, performed using ImageJ software, further supported these observations (Fig. 4D and F). Through the aforementioned series of experiments, it has been consistently demonstrated that activated platelet-derived vesicles exhibit optimal efficacy upon DOX delivery. This confirms that enhanced uptake is a critical step in the mechanism of action, providing key functionality for the *in vivo* capture of circulating tumor cells and the subsequent exertion of pharmacological effects.

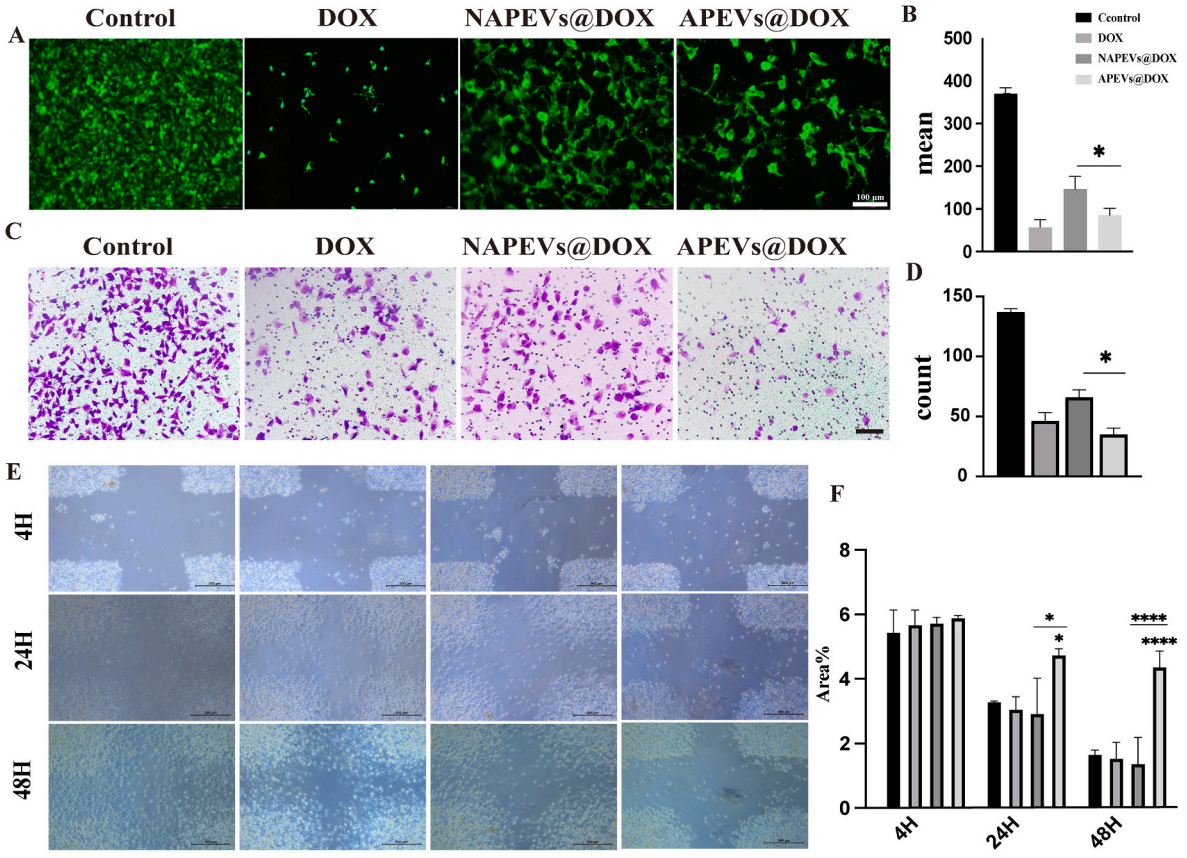

Fig. 4. *In vitro* cytotoxicity of APEVs@DOX. (A) The count of fluorescence microscopy images in MDA-MB-231 cells stained by Calcein AM. Scale bars: 50 μm. (B) Fluorescence quantification of the number of surviving cells in (A) graph by ImageJ software. (C) Representative images of invasive MDA-MB-231 tumor cells treated with saline, DOX, NAPEVs@DOX, APEVs@DOX in the Transwell invasion assay. Scale bar: 50 μm. (D) The data from the positive area in the Transwell assay were quantified using ImageJ. (E) Wound-healing assay. The Wound fields were photographed immediately after rinsing with PBS (0 h), and cell migration was photographed and documented for 48 h after administration of the different treatments, with representative images at 4, 24, and 48 h shown in Fig Scale bar: 200 μm. (F) Quantification of cell migration by ImageJ. Error bars are based on SD. *$p < 0.05$, **$p < 0.01$, ***$p < 0.001$, ****$p < 0.0001$.

3.5. *In vivo assessment of APEVs@DOX's targeting efficacy on circulating tumor cells and metastatic colonization in lung tissue*

Circulating tumor cells, defined as tumor cells present within the bloodstream, play a critical role in metastasis [12,42,43]. These cells often evade immune surveillance and resist mechanical stresses within the vasculature by forming complexes with platelets, erythrocytes, and fibrin, which can either shield them from immune attacks or promote their adhesion to the vessel walls [44,45]. Given the interaction dynamics between activated platelets and tumor cell surface receptors, we sought to explore the dynamic targeting capabilities of APEVs@DOX on CTCs *in vivo*.

In our experimental design, we mimicked the presence of CTCs in circulation by intravenously injecting tumor cells via the tail vein of mice. Prior to administration, MDA-MB-231-luci cells were labeled with green fluorescence using carboxyfluorescein succinimidyl ester (CFSE), while the doxorubicin in our biomimetic preparations emitted red fluorescence (DOX concentration, 5 mg/kg). Following dosing, whole blood samples were collected 4 h later, and erythrocytes were lysed to enable online examination of the co-localization status of the labeled cells and the APEVs@DOX via flow cytometry (Fig. 5A–C). Flow cytometric analysis revealed that tumor cells in the APEVs@DOX group exhibited a higher degree of co-localization with the preparation compared to those in the NAPEVs@DOX group, while there was no significant difference in co-localization ratio between DOX group and control group. This finding suggests that APEVs@DOX possess an enhanced affinity for circulating tumor cells, making it possible to deliver cytotoxic drugs to kill CTCs and inhibit the metastasis of tumor cells. In subsequent experiments, we were pleasantly surprised to find that APEVs@DOX not only exhibited good targeting towards circulating tumor cells, but also showed excellent targeting towards tumor cells that had metastasized to the lungs. We established a metastatic breast tumor model in nude mice using a tail vein injection of MDA-MB-231 tumor cells. After 24 h, we performed *in vivo* imaging and found that APEVs@DOX had the best targeting towards lung metastases(Fig. S9).

To further investigate the efficacy of the CTCs capturing strategy on the colonization and stasis of tumor cells within lung tissues, we established a CTCs model through tail vein injection in mice. Tumor cells were labeled with 5-chloromethylfluorescein diacetate (CMFDA)-SE prior to administration, and different drug treatments (DOX concentration, 3 mg/kg) were delivered via the tail vein. Frozen lung tissue sections obtained at 24 and 48 h post-injection were examined under a fluorescence microscope to monitor the colonization status of the tumor cells (Fig. 5D–F). The CMFDA-SE fluorescence served as a marker for the adhesion of tumor cells to the lung. As illustrated in Fig. 5D–F, tumor cells treated with APEVs@DOX displayed minimal aggregation and adhesion by more than 80 %. Notably, DOX group and NAPEVs@DOX only exhibited 26 % and 50 % inhibitory effect on the number of lung tumor cells colonized, indicating that the interaction with activated platelet membranes might contribute to the reduced seeding of metastatic tumors *in vivo*.

CTCs cells are a key factor in lung metastasis from triple-negative breast cancer, so we plan to further evaluate the efficacy of the agent on lung metastasis after the capture of CTCs *in vivo*. Then a short-term lung metastasis experiment was subsequently conducted to evaluate the suppressive effect of APEVs@DOX on tumor cell colonization within lung tissue. Following the completion of flow cytometry co-localization studies, blood samples were collected from the mice, which were then subjected to three consecutive administrations spaced one day apart. Sacrifice of the animals was carried out on the 10th and 20th days post-

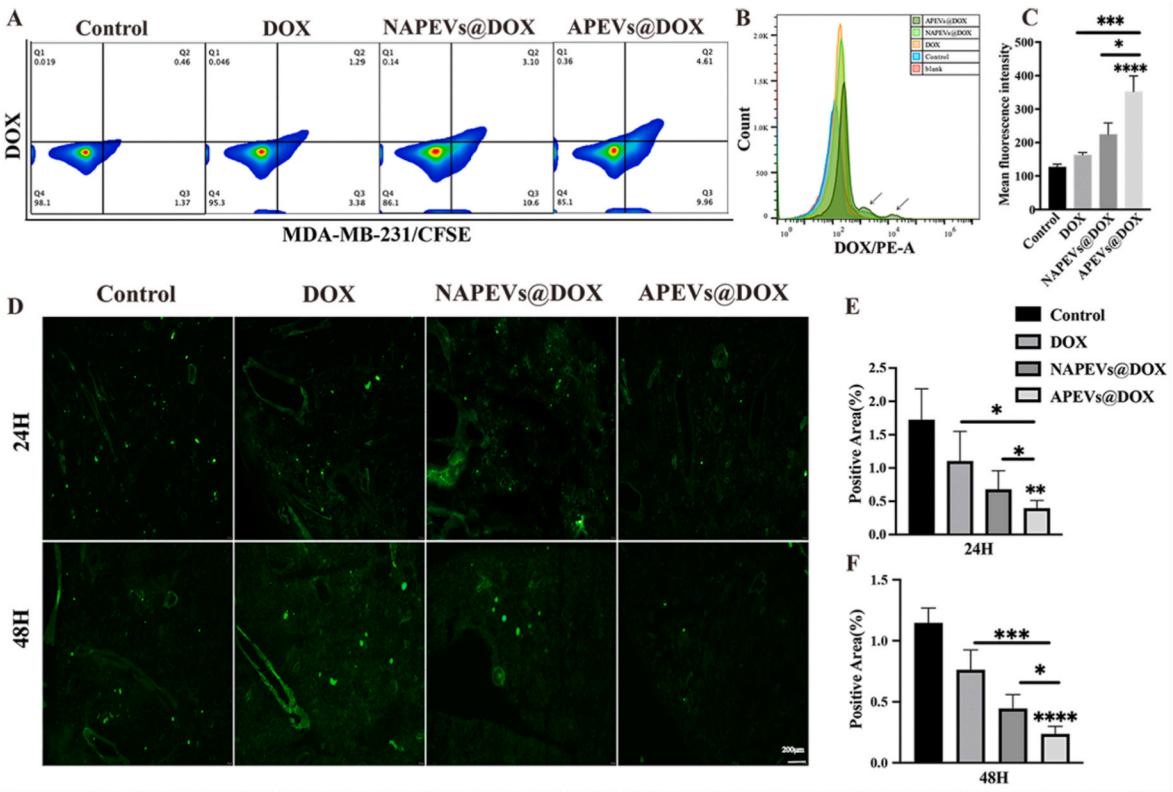

Fig. 5. Effect of APEVs@DOX on the targeting and colonization capabilities of CTCs *in vivo*. (A–C) Flow cytometry detection of fluorescence intensity of CFSE labeled tumor cells ingesting DOX treated with NAPEVs@DOX and APEVs@DOX in the circulation, and quantitative analysis of DOX fluorescence intensity. Error bars are based on SD. (D) Representative fluorescence images of frozen lung slices 24 and 48 h after intravenous administration of CFSE-labeled MDA-MB-231 cells pretreated with DOX, NAPEVs@DOX and APEVs@DOX Scale bar: 50 μm. (E–F) Fluorescence-positive areas of 24 h and 48 h CFSE were analyzed using ImageJ, respectively. Error bars are based on SD. *p < 0.05, **p < 0.01, ***p < 0.001,****p < 0.0001.

administration (Fig. 6A). On the 10th day, the area of pulmonary metastatic foci was measured using the small animal live imaging system and H&E staining sections. Tumor metastasis was observed in the lung tissues of all groups, but the APEVs@DOX group showed relatively fewer tumor metastases, and no obvious metastatic tumor nodules were found (Fig. 6B). On the 20th day, obvious tumor metastatic aggregation growth was observed in the lung tissues of the mice, but the APEVs@DOX treated group had relatively smaller tumor growth (Fig. 6C and Fig. S10), indicating that the constructed APEVs@DOX released doxorubicin to kill tumor cells and inhibit their metastatic growth after targeting and adhering to tumor cells. In brief, the data unequivocally demonstrates that both APEVs@DOX and NAPEVs@DOX exhibit pronounced anti-colonization effects against circulating tumor cells within the lung microenvironment. This efficacy is notably more pronounced compared to treatment with doxorubicin alone, which displays a relatively modest impact on CTCs colonization. The superior performance of APEVs@DOX can be attributed to its enhanced binding specificity towards tumor cells, as substantiated by our findings. Notably, following drugs administration in DOX free group, an unexpected metastasis promotion occurred, likely due to insufficient intracellular DOX levels in CTCs. This highlights the necessity for swift attainment of therapeutic drug concentrations to avoid resistance and metastasis facilitation. Clinicians and researchers should thus be vigilant against long-term low-dose therapy, which might inadvertently aid tumor spread. Optimal outcomes require time-sensitive, efficacious dosing strategies to promptly eliminate CTCs and minimize metastatic risk, crucial for chemotherapy protocol refinement [46–48].

To provide additional insight, the sequestration of doxorubicin within APEVs and NAPEVs appears to amplify its therapeutic window by precisely homing in on circulating tumor cells. This precision-targeting mechanism not only amplifies the cytotoxic potency of the drug specifically against neoplastic cells but also serves to minimize adverse side effects associated with non-specific biodistribution, thereby streamlining the therapeutic efficacy and safety profile. Particularly noteworthy is the pivotal function of platelets in facilitating tumor cell survival and escape from immune surveillance during the metastatic cascade. By adhering to and aggregating around CTCs, platelets create a protective barrier that shields these cells from immune system detection and destruction. The APEVs@DOX formulation, through its ability to inhibit CTCs activity and deplete surface-bound platelet receptors, effectively dismantles this protective shield. This action disrupts the platelet-mediated defense mechanisms, antagonizes platelet adhesion to CTCs, and diminishes the propensity of CTCs to colonize secondary sites, culminating in a marked suppression of metastatic spread. Thus, the APEVs@DOX construct not only represents an innovative approach to enhancing chemotherapy effectiveness but also underscores the importance of disrupting the intricate interplay between platelets and CTCs in the metastatic process. This strategy holds promise for advancing the clinical management of metastatic disease by specifically targeting mechanisms that contribute to tumor cell survival and dissemination.

3.6. *Therapeutic efficacy of APEVs@DOX on breast cancer lung metastasis in vivo*

Given the lung's predilection as a metastatic site for breast cancer cells, the tail vein injection model using MDA-MB-231 tumor cells was utilized to establish a metastatic breast tumor *in vivo*. As shown in Fig. 7A, female BALB/c nude mice carrying CTCs were administered different formulations (DOX concentration, 3 mg/kg) every 2 days, for a total of 7 injections. The cytotoxicity of APEVs@DOX was assessed by measuring the weight changes of the mice throughout the study period. The analysis showed that there were no significant changes in the weight of the mice in each group during the treatment process (Fig. 7B). At the end of the experiment, lungs and other organs from each group were collected, and metastatic nodules in the lungs were observed and recorded by gross examination. The results showed that histological H&E staining assessment indicated extensive tumor burden in the lung tissues of the control group. Compared with the PBS control group, both the DOX group and the NAPEVs@DOX group exhibited similar tumor burdens, while the formation of pulmonary the formation of pulmonary metastatic foci was moderately reduced under the treatment of APEVs@DOX, with only clusters of cells with deeply stained nuclei visible (Fig. 7C and D). The histological H&E staining of other organs and the results of liver function test showed no significant organ damage, further proving the safety of the drug (Figs. S11 and S12).

Furthermore, Tunel assays conducted on lung tissue sections revealed the highest level of apoptosis in the metastatic lung tissue of the APEVs@DOX group. This finding underscores the efficacy of the APEVs@DOX system in specifically targeting and inhibiting the progression of formed lung metastasis niche. Moreover,

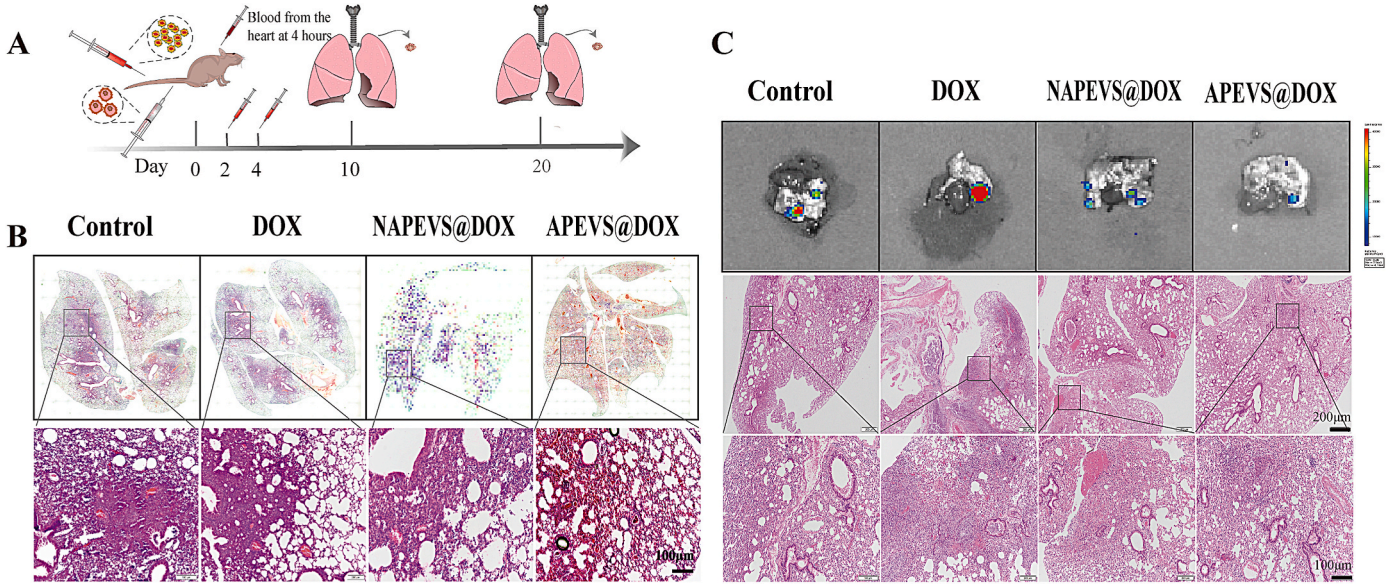

Fig. 6. (A) Schematic diagram of the *in vivo* anti-CTCs colonization and growth assay process; (B) Mice were sacrificed 10 days after tail vein injection of tumor cells and different treatment, while lung tissue was photographed by bioluminescence imaging as well as H&E staining of tissue sections and regional enlargements respectively; (C) H&E staining of mouse lung sections at 20 days.

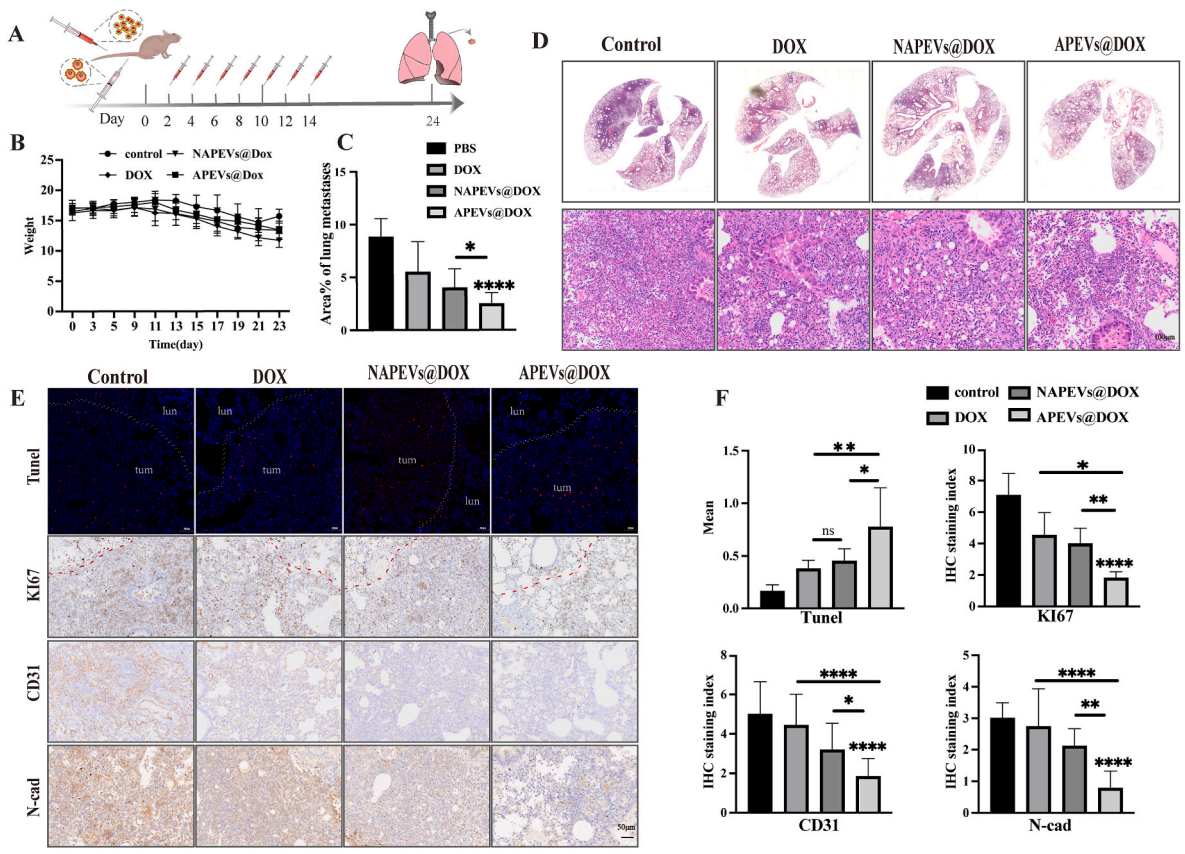

Fig. 7. *In vivo* experiments. (A) Schematic illustrating APEVs@DOX antitumor metastasis therapy. (B) Body weight change curves in mice for various treatment groups. (C) Quantification of the area of lung metastases. (D) Representative lung tissue sections with HE staining photographed and local magnification. (E) Representative images of Tunel-stained lung, Ki67, CD31, and N-cad in different treatments. Scale bar: 50 μm. (F) Corresponding IHC staining apoptosis index of Tunel and proliferation index of Ki67, CD31, and N-cad in different groups. Error bars are based on SD. *p < 0.05, **p < 0.01, ***p < 0.001,****p < 0.0001.

immunohistochemical analysis indicated a significant decrease in the expression of the cytoskeletal protein N-cadherin and the proliferative marker Ki67 in the APEVs@DOX injected group compared to the controls. Angiogenesis is a crucial factor in promoting tumor metastasis, and tumor vessels were identified by staining with the mouse endothelial cell marker CD31. As shown in the figure, vessel density in the APEVs@DOX group was relatively lower than that in the control group, implying a reduction in angiogenesis(Fig. 7E). In addition, in the Tunel immunostaining of lung tissue, there was no statistically significant difference in the quantification of apoptotic cells between the DOX group and the NAPEVs@DOX group compared to the PBS control group. The immunohistochemical staining results showed that these two groups had similar expressions of Ki67, CD31, and N-cad. The aforementioned pathological results were quantified semiquantitatively using ImageJ software (Fig. 7F), providing numerical evidence of the treatment's impact. Collectively, these findings suggest that APEVs@DOX treatment can effectively target CTCs and holds promise in significantly mitigating breast cancer lung metastasis. Beyond the targeted elimination of circulating tumor cells to curb metastasis, APEVs@DOX exerts an inhibitory effect on the proliferation of already established metastatic foci due to its high affinity for tumor cells. This dual mechanism synergistically contributes to the suppression of lung metastasis in the context of breast cancer, showcasing the comprehensive anti-metastatic potential of APEVs@DOX.

4. Conclusion

Our research focused on developing APEVs@DOX, a targeted therapeutic strategy for triple-negative breast cancer (TNBC) metastasis. By engineering vesicles coated with activated platelet membranes and loaded with doxorubicin, we aimed to exploit the unique interaction between CTCs and platelets. This interaction is known to protect CTCs from immune surveillance and promote their survival during dissemination. Our results showed that APEVs@DOX had enhanced binding affinity to CTCs compared to inactivated platelet-derived vesicles or free doxorubicin. This selective targeting allowed efficient delivery of doxorubicin directly to CTCs, inhibiting their survival and proliferation. Additionally, APEVs@DOX disrupted the protective mechanisms of platelets, reducing CTCs colonization in secondary sites. In a TNBC lung metastasis model, APEVs@DOX significantly reduced metastatic nodules and increased apoptosis in metastatic lung tissue. Immunohistochemical analysis revealed decreased expression of N-cadherin and Ki67, indicating reduced cell motility and proliferation. APEVs@DOX also decreased angiogenesis, as evidenced by lower vessel density in metastatic tissue compared to controls. Importantly, APEVs@DOX did not induce significant systemic toxicity. This study demonstrates a novel approach to targeting CTCs by leveraging their interaction with platelets, offering a potential strategy for improving TNBC treatment by specifically targeting mechanisms that support tumor cell survival and dissemination.

CRediT authorship contribution statement

Hongmei Zhang: Writing – original draft, Validation, Methodology, Formal analysis. **Jinlan Jiao:** Writing – original draft, Validation, Methodology, Formal analysis. **Yongxuan Long:** Writing – original draft, Validation, Methodology, Formal analysis. **Lina Zhou:** Writing – original draft, Investigation. **Yinhua Lv:** Writing – original draft, Investigation. **Wenqian Wei:** Writing – original draft, Investigation. **Yuxiang Sun:** Writing – original draft, Investigation. **Hao Han:** Writing

– original draft, Investigation. **Changrong Chen:** Supervision, Resources, Project administration, Funding acquisition, Conceptualization. **Yun Zhu:** Supervision, Resources, Project administration, Funding acquisition, Conceptualization. **Weijie Zhang:** Supervision, Resources, Project administration, Funding acquisition, Conceptualization.

Funding

This work was supported by the National Natural Science Foundation of China (82102917, 81672380), Nanjing Special Foundation for Health Science and Technology Development (ZKX23012, YKK23104), and Crosswise Project of Nanjing University (No. 2020-K001).

Declaration of competing interest

The authors declare that they have no known competing financial interests or personal relationships that could have appeared to influence the work reported in this paper.

Acknowledgement

None.

Appendix A. Supplementary data

Supplementary data to this article can be found online at https://doi.org/10.1016/j.mtbio.2025.101597.

Data availability

Data will be made available on request.

References

[1] R. Lawrence, M. Watters, C.R. Davies, K. Pantel, Y.-J. Lu, Circulating tumour cells for early detection of clinically relevant cancer, Nat. Rev. Clin. Oncol. 20 (2023) 487–500, https://doi.org/10.1038/s41571-023-00781-y.

[2] R.A. Leon-Ferre, M.P. Goetz, Advances in systemic therapies for triple negative breast cancer, BMJ 381 (2023) e071674, https://doi.org/10.1136/bmj-2022-071674.

[3] S. Lei, R. Zheng, S. Zhang, S. Wang, R. Chen, K. Sun, H. Zeng, J. Zhou, W. Wei, Global patterns of breast cancer incidence and mortality: a population-based cancer registry data analysis from 2000 to 2020, Cancer Commun. 41 (2021) 1183–1194, https://doi.org/10.1002/cac2.12207.

[4] J. Qi, M. Li, L. Wang, Y. Hu, W. Liu, Z. Long, Z. Zhou, P. Yin, M. Zhou, National and subnational trends in cancer burden in China, 2005-20: an analysis of national mortality surveillance data, Lancet Public Health 8 (2023) e943–e955, https://doi.org/10.1016/S2468-2667(23)00211-6.

[5] Z. Deng, S. Wu, Y. Wang, D. Shi, Circulating tumor cell isolation for cancer diagnosis and prognosis, EBioMedicine 83 (2022) 104237, https://doi.org/10.1016/j.ebiom.2022.104237.

[6] E. Schuster, R. Taftaf, C. Reduzzi, M.K. Albert, I. Romero-Calvo, H. Liu, Better together: circulating tumor cell clustering in metastatic cancer, Trends Cancer 7 (2021) 1020–1032, https://doi.org/10.1016/j.trecan.2021.07.001.

[7] F. Castro-Giner, N. Aceto, Tracking cancer progression: from circulating tumor cells to metastasis, Genome Med. 12 (2020) 31, https://doi.org/10.1186/s13073-020-00728-3.

[8] A. Tr, A case of cancer in which cells similar to those in the tumours were seen in the blood after death, Australas. Med. J. 14 (1869) 146.

[9] S. Riethdorf, V. Müller, S. Loibl, V. Nekljudova, K. Weber, J. Huober, T. Fehm, I. Schrader, J. Hilfrich, F. Holms, H. Tesch, C. Schem, G. Von Minckwitz, M. Untch, K. Pantel, Prognostic impact of circulating tumor cells for breast cancer patients treated in the neoadjuvant "Geparquattro" trial, Clin. Cancer Res. 23 (2017) 5384–5393, https://doi.org/10.1158/1078-0432.CCR-17-0255.

[10] F.-C. Bidard, S. Michiels, S. Riethdorf, V. Mueller, L.J. Esserman, A. Lucci, B. Naume, J. Horiguchi, R. Gisbert-Criado, S. Sleijfer, M. Toi, J.A. Garcia-Saenz, A. Hartkopf, D. Generali, F. Rothé, J. Smerage, L. Muinelo-Romay, J. Stebbing, P. Viens, M.J.M. Magbanua, C.S. Hall, O. Engebraaten, D. Takata, J. Vidal-Martínez, W. Onstenk, N. Fujisawa, E. Diaz-Rubio, F.-A. Taran, M.R. Cappelletti, M. Ignatiadis, C. Proudhon, D.M. Wolf, J.B. Bauldry, E. Borgen, R. Nagaoka, V. Carañana, J. Kraan, M. Maestro, S.Y. Brucker, K. Weber, F. Reyal, D. Amara, M. G. Karhade, R.R. Mathiesen, H. Tokiniwa, A. Llombart-Cussac, A. Meddis, P. Blanche, K. d'Hollander, P. Cottu, J.W. Park, S. Loibl, A. Latouche, J.-Y. Pierga, K. Pantel, Circulating tumor cells in breast cancer patients treated by neoadjuvant chemotherapy: a meta-analysis, JNCI J. Natl. Cancer Inst. 110 (2018) 560–567, https://doi.org/10.1093/jnci/djy018.

[11] E. Trapp, W. Janni, C. Schindlbeck, J. Jückstock, U. Andergassen, A. De Gregorio, M. Alunni-Fabbroni, M. Tzschaschel, A. Polasik, J.G. Koch, T.W.P. Friedl, P. A. Fasching, L. Haeberle, T. Fehm, A. Schneeweiss, M.W. Beckmann, K. Pantel, V. Mueller, B. Rack, C. Scholz, SUCCESS Study Group, Presence of circulating tumor cells in high-risk early breast cancer during follow-up and prognosis, JNCI J. Natl. Cancer Inst. 111 (2019) 380–387, https://doi.org/10.1093/jnci/djy152.

[12] D. Lin, L. Shen, M. Luo, K. Zhang, J. Li, Q. Yang, F. Zhu, D. Zhou, S. Zheng, Y. Chen, J. Zhou, Circulating tumor cells: biology and clinical significance, Signal Transduct. Targeted Ther. 6 (2021) 404, https://doi.org/10.1038/s41392-021-00817-8.

[13] K. Wang, H. Ye, X. Zhang, X. Wang, B. Yang, C. Luo, Z. Zhao, J. Zhao, Q. Lu, H. Zhang, Q. Kan, Y. Wang, Z. He, J. Sun, An exosome-like programmable-bioactivating paclitaxel prodrug nanoplatform for enhanced breast cancer metastasis inhibition, Biomaterials 257 (2020) 120224, https://doi.org/10.1016/j.biomaterials.2020.120224.

[14] K. Morris, B. Schnoor, A.-L. Papa, Platelet cancer cell interplay as a new therapeutic target, Biochim. Biophys. Acta BBA - Rev. Cancer 1877 (2022) 188770, https://doi.org/10.1016/j.bbcan.2022.188770.

[15] M. Schlesinger, Role of platelets and platelet receptors in cancer metastasis, J. Hematol. Oncol.J Hematol Oncol 11 (2018) 125, https://doi.org/10.1186/s13045-018-0669-2.

[16] F. Gaertner, S. Massberg, Patrolling the vascular borders: platelets in immunity to infection and cancer, Nat. Rev. Immunol. 19 (2019) 747–760, https://doi.org/10.1038/s41577-019-0202-z.

[17] D.H. Liang, C. Hall, A. Lucci, Circulating tumor cells in breast cancer, Recent Results Cancer Res. Fortschritte Krebsforsch. Progres Dans Rech. Sur Cancer 215 (2020) 127–145, https://doi.org/10.1007/978-3-030-26439-0_7.

[18] R.H. Fang, W. Gao, L. Zhang, Targeting drugs to tumours using cell membrane-coated nanoparticles, Nat. Rev. Clin. Oncol. 20 (2023) 33–48, https://doi.org/10.1038/s41571-022-00699-x.

[19] D. Zou, Z. Wu, X. Yi, Y. Hui, G. Yang, Y. Liu, Tengjisi, H. Wang, A. Brooks, H. Wang, X. Liu, Z.P. Xu, M.S. Roberts, H. Gao, C.-X. Zhao, Nanoparticle elasticity regulates the formation of cell membrane-coated nanoparticles and their nano-bio interactions, Proc. Natl. Acad. Sci. 120 (2023) e2214757120, https://doi.org/10.1073/pnas.2214757120.

[20] Z. Chen, P. Zhao, Z. Luo, M. Zheng, H. Tian, P. Gong, G. Gao, H. Pan, L. Liu, A. Ma, H. Cui, Y. Ma, L. Cai, Cancer cell membrane-biomimetic nanoparticles for homologous-targeting dual-modal imaging and photothermal therapy, ACS Nano 10 (2016) 10049–10057, https://doi.org/10.1021/acsnano.6b04695.

[21] X. Fan, K. Wang, Q. Lu, Y. Lu, F. Liu, L. Li, S. Li, H. Ye, J. Zhao, L. Cao, H. Zhang, Z. He, J. Sun, Surface-anchored tumor microenvironment-responsive protein nanogel-platelet system for cytosolic delivery of therapeutic protein in the post-surgical cancer treatment, Acta Biomater. 154 (2022) 412–423, https://doi.org/10.1016/j.actbio.2022.10.031.

[22] Q. Lu, H. Ye, K. Wang, J. Zhao, H. Wang, J. Song, X. Fan, Y. Lu, L. Cao, B. Wan, H. Zhang, Z. He, J. Sun, Bioengineered platelets combining chemotherapy and immunotherapy for postsurgical melanoma treatment: internal core-loaded doxorubicin and external surface-anchored anti-PD-L1 antibody backpacks, Nano Lett. 22 (2022) 3141–3150, https://doi.org/10.1021/acs.nanolett.2c00907.

[23] J. Zhao, H. Ye, Q. Lu, K. Wang, X. Chen, J. Song, H. Wang, Y. Lu, M. Cheng, Z. He, Y. Zhai, H. Zhang, J. Sun, Inhibition of post-surgery tumour recurrence via a sprayable chemo-immunotherapy gel releasing PD-L1 antibody and platelet-derived small EVs, J. Nanobiotechnol. 20 (2022) 62, https://doi.org/10.1186/s12951-022-01270-7.

[24] R. Edgar, Gene Expression Omnibus: NCBI gene expression and hybridization array data repository, Nucleic Acids Res. 30 (2002) 207–210, https://doi.org/10.1093/nar/30.1.207.

[25] D. Huang, B.T. Sherman, Q. Tan, J.R. Collins, W.G. Alvord, J. Roayaei, R. Stephens, M.W. Baseler, H.C. Lane, R.A. Lempicki, The DAVID Gene Functional Classification Tool: a novel biological module-centric algorithm to functionally analyze large gene lists, Genome Biol. 8 (2007) R183, https://doi.org/10.1186/gb-2007-8-9-r183.

[26] M. Ashburner, C.A. Ball, J.A. Blake, D. Botstein, H. Butler, J.M. Cherry, A.P. Davis, K. Dolinski, S.S. Dwight, J.T. Eppig, M.A. Harris, D.P. Hill, L. Issel-Tarver, A. Kasarskis, S. Lewis, J.C. Matese, J.E. Richardson, M. Ringwald, G.M. Rubin, G. Sherlock, Gene ontology: tool for the unification of biology. The Gene Ontology Consortium, Nat. Genet. 25 (2000) 25–29, https://doi.org/10.1038/75556.

[27] A. Franceschini, D. Szklarczyk, S. Frankild, M. Kuhn, M. Simonovic, A. Roth, J. Lin, P. Minguez, P. Bork, C. von Mering, L.J. Jensen, STRING v9.1: protein-protein interaction networks, with increased coverage and integration, Nucleic Acids Res 41 (2013) D808–D815, https://doi.org/10.1093/nar/gks1094.

[28] M.E. Smoot, K. Ono, J. Ruscheinski, P.-L. Wang, T. Ideker, Cytoscape 2.8: new features for data integration and network visualization, Bioinformatics 27 (2011) 431–432, https://doi.org/10.1093/bioinformatics/btq675.

[29] Y. Xiong, Z. Liu, Z. Li, S. Wang, N. Shen, Y. Xin, T. Huang, Long non-coding RNA nuclear paraspeckle assembly transcript 1 interacts with microRNA-107 to modulate breast cancer growth and metastasis by targeting carnitine palmitoyltransferase-1, Int. J. Oncol. 55 (2019) 1125–1136, https://doi.org/10.3892/ijo.2019.4869.

[30] T. Pereira-Veiga, S. Schneegans, K. Pantel, H. Wikman, Circulating tumor cell-blood cell crosstalk: biology and clinical relevance, Cell Rep. 40 (2022) 111298, https://doi.org/10.1016/j.celrep.2022.111298.

[31] H.G. Roweth, E.M. Battinelli, Lessons to learn from tumor-educated platelets, Blood 137 (2021) 3174–3180, https://doi.org/10.1182/blood.2019003976.

[32] X. Liu, J. Song, H. Zhang, X. Liu, F. Zuo, Y. Zhao, Y. Zhao, X. Yin, X. Guo, X. Wu, H. Zhang, J. Xu, J. Hu, J. Jing, X. Ma, H. Shi, Immune checkpoint HLA-E:CD94-

NKG2A mediates evasion of circulating tumor cells from NK cell surveillance, Cancer Cell 41 (2023) 272–287.e9, https://doi.org/10.1016/j.ccell.2023.01.001.
[33] Y. Sun, T. Li, L. Ding, J. Wang, C. Chen, T. Liu, Y. Liu, Q. Li, C. Wang, R. Huo, H. Wang, T. Tian, C. Zhang, B. Pan, J. Zhou, J. Fan, X. Yang, W. Yang, B. Wang, W. Guo, Platelet-mediated circulating tumor cell evasion from natural killer cell killing through immune checkpoint CD155-TIGIT, Hepatology (2024), https://doi.org/10.1097/HEP.0000000000000934.
[34] D.L. Tao, S. Tassi Yunga, C.D. Williams, O.J.T. McCarty, Aspirin and antiplatelet treatments in cancer, Blood 137 (2021) 3201–3211, https://doi.org/10.1182/blood.2019003977.
[35] M. Malehmir, D. Pfister, S. Gallage, M. Szydlowska, D. Inverso, E. Kotsiliti, V. Leone, M. Peiseler, B.G.J. Surewaard, D. Rath, A. Ali, M.J. Wolf, H. Drescher, M. E. Healy, D. Dauch, D. Kroy, O. Krenkel, M. Kohlhepp, T. Engleitner, A. Olkus, T. Sijmonsma, J. Volz, C. Deppermann, D. Stegner, P. Helbling, C. Nombela-Arrieta, A. Rafiei, M. Hinterleitner, M. Rall, F. Baku, O. Borst, C.L. Wilson, J. Leslie, T. O'Connor, C.J. Weston, A. Chauhan, D.H. Adams, L. Sheriff, A. Teijeiro, M. Prinz, R. Bogeska, N. Anstee, M.N. Bongers, M. Notohamiprodjo, T. Geisler, D. J. Withers, J. Ware, D.A. Mann, H.G. Augustin, A. Vegiopoulos, M.D. Milsom, A. J. Rose, P.F. Lalor, J.M. Llovet, R. Pinyol, F. Tacke, R. Rad, M. Matter, N. Djouder, P. Kubes, P.A. Knolle, K. Unger, L. Zender, B. Nieswandt, M. Gawaz, A. Weber, M. Heikenwalder, Platelet GPIbα is a mediator and potential interventional target for NASH and subsequent liver cancer, Nat. Med. 25 (2019) 641–655, https://doi.org/10.1038/s41591-019-0379-5.
[36] L.A. Coupland, B.H. Chong, C.R. Parish, Platelets and P-selectin control tumor cell metastasis in an organ-specific manner and independently of NK cells, Cancer Res. 72 (2012) 4662–4671, https://doi.org/10.1158/0008-5472.CAN-11-4010.
[37] L.L. Coelho, M.M. Vianna, D.M. Da Silva, B.M.D.S. Gonzaga, R.R. Ferreira, A. C. Monteiro, A.C. Bonomo, P.P.D.A. Manso, M.A. De Carvalho, F.R. Vargas, L. R. Garzoni, Spheroid model of mammary tumor cells: epithelial–mesenchymal transition and doxorubicin response, Biology 13 (2024) 463, https://doi.org/10.3390/biology13070463.
[38] C.M. Cardador, T.B. De Castro, R.J.A. De Castro, A.L. Bocca, L.C. Camargo, T. A. Pacheco, L.A. Muehlmann, J.P.F. Longo, Doxorubicin-induced immunogenic cell death impairs tumor progression and distant metastasis in a 4T1 breast cancer tumor model, Curr. Pharm. Des. 30 (2024) 2493–2504, https://doi.org/10.2174/0113816128316870240610045550.
[39] I. Pastushenko, C. Blanpain, EMT transition states during tumor progression and metastasis, Trends Cell Biol. 29 (2019) 212–226, https://doi.org/10.1016/j.tcb.2018.12.001.
[40] Y. Huang, W. Hong, X. Wei, The molecular mechanisms and therapeutic strategies of EMT in tumor progression and metastasis, J. Hematol. Oncol.J Hematol Oncol 15 (2022) 129, https://doi.org/10.1186/s13045-022-01347-8.
[41] Y. Zhang, J.L. Donaher, S. Das, X. Li, F. Reinhardt, J.A. Krall, A.W. Lambert, P. Thiru, H.R. Keys, M. Khan, M. Hofree, M.M. Wilson, O. Yedier-Bayram, N. A. Lack, T.T. Onder, T. Bagci-Onder, M. Tyler, I. Tirosh, A. Regev, J.A. Lees, R. A. Weinberg, Genome-wide CRISPR screen identifies PRC2 and KMT2D-COMPASS as regulators of distinct EMT trajectories that contribute differentially to metastasis, Nat. Cell Biol. 24 (2022) 554–564, https://doi.org/10.1038/s41556-022-00877-0.
[42] M. Yu, A. Bardia, B.S. Wittner, S.L. Stott, M.E. Smas, D.T. Ting, S.J. Isakoff, J. C. Ciciliano, M.N. Wells, A.M. Shah, K.F. Concannon, M.C. Donaldson, L.V. Sequist, E. Brachtel, D. Sgroi, J. Baselga, S. Ramaswamy, M. Toner, D.A. Haber, S. Maheswaran, Circulating breast tumor cells exhibit dynamic changes in epithelial and mesenchymal composition, Science 339 (2013) 580–584, https://doi.org/10.1126/science.1228522.
[43] S. Gkountela, F. Castro-Giner, B.M. Szczerba, M. Vetter, J. Landin, R. Scherrer, I. Krol, M.C. Scheidmann, C. Beisel, C.U. Stirnimann, C. Kurzeder, V. Heinzelmann-Schwarz, C. Rochlitz, W.P. Weber, N. Aceto, Circulating tumor cell clustering shapes DNA methylation to enable metastasis seeding, Cell 176 (2019) 98–112.e14, https://doi.org/10.1016/j.cell.2018.11.046.
[44] N.K. Dashzeveg, Y. Jia, Y. Zhang, L. Gerratana, P. Patel, A. Shajahan, T. Dandar, E. K. Ramos, H.F. Almubarak, V. Adorno-Cruz, R. Taftaf, E.J. Schuster, D. Scholten, M.T. Sokolowski, C. Reduzzi, L. El-Shennawy, A.D. Hoffmann, M. Manai, Q. Zhang, P. D'Amico, P. Azadi, K.J. Colley, L.C. Platanias, A.N. Shah, W.J. Gradishar, M. Cristofanilli, W.A. Muller, B.A. Cobb, H. Liu, Dynamic glycoprotein hyposialylation promotes chemotherapy evasion and metastatic seeding of quiescent circulating tumor cell clusters in breast cancer, Cancer Discov. 13 (2023) 2050–2071, https://doi.org/10.1158/2159-8290.CD-22-0644.
[45] A. Gvozdenovic, N. Aceto, Metastasis unleashed: hyposialylation empowers chemo-evasive circulating tumor cell clusters in breast cancer, Cancer Res. 83 (2023) 2811–2812, https://doi.org/10.1158/0008-5472.CAN-23-1978.
[46] L. Monteran, N. Ershaid, H. Doron, Y. Zait, Y. Scharff, S. Ben-Yosef, C. Avivi, I. Barshack, A. Sonnenblick, N. Erez, Chemotherapy-induced complement signaling modulates immunosuppression and metastatic relapse in breast cancer, Nat. Commun. 13 (2022) 5797, https://doi.org/10.1038/s41467-022-33598-x.
[47] I. Keklikoglou, C. Cianciaruso, E. Güç, M.L. Squadrito, L.M. Spring, S. Tazzyman, L. Lambein, A. Poissonnier, G.B. Ferraro, C. Baer, A. Cassará, A. Guichard, M. L. Iruela-Arispe, C.E. Lewis, L.M. Coussens, A. Bardia, R.K. Jain, J.W. Pollard, M. De Palma, Chemotherapy elicits pro-metastatic extracellular vesicles in breast cancer models, Nat. Cell Biol. 21 (2019) 190–202, https://doi.org/10.1038/s41556-018-0256-3.
[48] G.S. Karagiannis, J.M. Pastoriza, Y. Wang, A.S. Harney, D. Entenberg, J. Pignatelli, V.P. Sharma, E.A. Xue, E. Cheng, T.M. D'Alfonso, J.G. Jones, J. Anampa, T. E. Rohan, J.A. Sparano, J.S. Condeelis, M.H. Oktay, Neoadjuvant chemotherapy induces breast cancer metastasis through a TMEM-mediated mechanism, Sci. Transl. Med. 9 (2017) eaan0026, https://doi.org/10.1126/scitranslmed.aan0026.